Coupling of Volume of Fluid and Level Set Methods in Condensing Heat Transfer Simulations

R. Kahraman[a], D. Bacheva[a], A. Schmieder[a] and G. R. Tabor[b]

[a]HiETA Technologies Ltd, Bristol and Bath Science Park, Dirac Crescent, BS16 7FR, UK; [b]College of Engineering, Mathematics and Physical Sciences, University of Exeter, North Park Road, Exeter EX4 4QF, UK

ARTICLE HISTORY
Compiled December 18, 2020

ABSTRACT
Additive Manufacturing (AM) is a rapidly developing new technology which allows the manufacture of arbitrarily complex geometries, and which is likely to transform heat exchanger design. To drive this transformation we need to develop computer modelling techniques to model fluid flow, heat exchange and phase change in arbitrarily complex domains, such as can be manufactured using AM. The present work aims to develop a computational fluid dynamics (CFD) model for heat transfer and phase change, robust enough to model compact AM heat exchangers for automotive fuel cell application. The hydrodynamics of the two-phase flow is captured via the Volume Of Fluid (VOF) approach, coupled with a Level Set method in order to capture the sharp interface between liquid and vapour in laminar film condensation. The Stefan problem is used to show the improvement of the interface tracking with LS-VOF against VOF approach. The resulting complete condensation model is applied for the first time for a complex AM geometry and validated against experimental data.

KEYWORDS
CFD, OpenFOAM, Volume of Fluid, Level Set, Condensation, Heat Transfer, Heat Exchanger

Nomenclature

C	compression coefficient, [−]
C_p	specific heat capacity, [J/kgK]
F	interface induced volume force, [N/m^3]
g	gravity, [m/s^2]
h	latent heat, [J/kg]
S	source term, [kg/m^3 s]
T	temperature, [K]
t	time, [s]
U	mean velocity, [m/s]
α	volume fraction, [−]
δ	interface position, [m]
ϵ	interface thickness, [m]
Γ	characteristic cell size, [−]

κ	interface curvature, [1/m]
λ	thermal conductivity, [W/mK]
μ	dynamic viscosity, [Pa s]
ϕ	level set function, [−]
ρ	density, [kg/m^3]
σ	surface tension coefficient, [m]
τ	artificial dimensionless time, [−]
D	diameter, [m]
0	initial value
c	compression
eff	mixture effective
h	heat source
l	liquid
m	mixture
sat	saturated
v	vapour
w	wall

1. Introduction

The development of compact heat exchangers is important for automotive, aerospace and space technology applications. Compact heat exchangers can improve efficiency, reduce weight and optimise the usage of space, all of which are important considerations in these areas. This is particularly the case for the automotive industry, in which fuel cells are being seriously investigated as an alternative to conventional combustion engines and power plants. Fuel cells generate electricity directly through chemical reaction, generating water vapour as an exhaust, and this exhaust has to be cooled to condense out the water component. The more efficient and light-weight this heat exchanger is, the greater the overall power plant efficiency.

Additive Manufacturing (AM) is the name given to a number of rapidly developing manufacturing technologies in which a part is built up layer by layer through some form of deposition process. Examples include fused deposition, in which layers of powder (typically metal or plastic) are laid down and fused together using lasers, and 3D printing in which a fast-setting material (typically a plastic) is extruded from a mobile printing head to build up each layer. However it is achieved, AM enables the direct fabrication of a part from a CAD design. Advantages of the technique can include a lower material wastage rate, the ability to customise components easily, and the ability to manufacture a wider range of geometric structures, including structures which could not possibly be manufactured by traditional subtractive manufacturing, injection moulding, or other more conventional approaches. This last is the driving impetus towards applying AM techniques to heat exchanger design. A conventional heat exchanger might comprise a few tubes, scale of cm or larger, welded together. AM provides the possibility of creating designs with hundreds of fine tubes with complex geometries (spiral, helical, expanding/contracting) connected through optimised inlet and outlet manifolds. The small scale of the tubes implies a high surface area of contact for heat exchange, and whatever geometry is calculated to be required can be manufactured. In order to design the AM heat exchanger we need to have a computational model to predict and optimise fluid flow, heat exchange and phase change, and this computational model needs to be sufficiently robust to be able to deal with

the highly complex geometries which can be produced with AM. The purpose of this paper is to present for the first time a CFD model which is sufficiently advanced that it is able to simulate all these physical effects, and sufficiently robust that it is able to cope with the arbitrarily complex geometries which can be manufactured with AM methods.

1.1. *Multiphase flow*

Computational Fluid Dynamics (CFD) is the use of computers to solve the governing equations of fluid dynamics, often on complex 3D domains. These governing equations start with the Navier-Stokes equations, or for turbulent flow, averaged equations derived from these equations, but can also include equations for heat transfer, species concentration dynamics, multiphase flow and phase change. In the current paper we are interested in simulating condensing heat exchangers. This requires us to solve a multiphase flow problem to model the dynamics of both the air/water vapour phase and the liquid water phase, as well as the change in phase of water vapour to liquid water and the resultant energy release from the latent heat of condensation. Both Eulerian dispersed phase and interface-capturing free surface methods have been used to model boiling and condensation phenomena, depending on whether the condensed phase forms dispersed sub-grid-scale droplets or larger contiguous regions of fluid. The Eulerian dispersed phase approach (Rusche 2002), in which interpenetrating sets of immiscible phases are modelled by separate dynamical equations together with a volume fraction α to represent the fraction of each cell occupied by one of the phases, is applicable for cases where numerous small droplets are being formed. The alternative interface-capturing methods (Ubbink and Issa 1999) are applied for free surface flows where a macroscopic interface needs to be resolved as part of the simulation; hence they are used for smooth annular, wavy annular and macro scale droplet flows. The most famous interface capturing methods are the Volume of Fluid (VOF) (Ubbink and Issa 1999) and Level Set (LS) (Albadawi et al. 2013; Sussman and Puckett 2000; Osher and Fedkiw 2001) methods, in which some form of indicator function is solved to identify which phase is which, and from which the location of the interface can be derived. In VOF modelling, the indicator function takes values between 0 (fluid A) and 1 (fluid B), and the location of the interface is indicated where the values are between these extremes. In LS methods the indicator function ranges between positive and negative values, and the location of the interface is identified with an indicator function value of 0. Because of its simplicity and flexibility, Volume of Fluid (VOF) method (Ubbink and Issa 1999; Anderson 1982; Hirt and Nichols 1981) has been used in many applications of multiphase modelling; in particular it conserves the mass in each phase (in the absence of any explicit model to transfer mass from one to the other). However the location of the interface is not completely determined and is subject to smearing across 2-3 cells in the mesh, which can be detrimental when modelling the surface tension which is crucial for interface resolving film condensation. Significant effort has been put into developing numerical and modelling approaches to sharpen the interface for this and other reasons. In addition to this, the surface tension needs to be calculated, and this can cause numerical problems as well. The surface tension, included as a source term in the momentum equation, is calculated using the Continuum Surface Force (CSF) model (Brackbill et al. 1992) which relies on approximation of the interface curvature gradient of the VOF function. Numerical errors in the representation of the indicator function in the region of the interface can

lead to slight errors in the evaluation of the surface normal vector and thus in the development of spurious currents (Parasitic currents) on the interface (Harvie et al. 2006).

The LS method was first introduced by Osher and Sethian (1988) and then implemented for multiphase flow by Sussman et al. (1994). Here, a function ϕ is introduced for which $\phi = 0$ represents the location of the interface; with $\phi < 0$ in one distinct phase and $\phi > 0$ in the other. At least close to the interface, ϕ can be taken as a measure of the distance to the interface. In contrast to VOF, the LS method does not guarantee conservation of the phases. However it does have a unique definition of ϕ for the interface which provides a sharp interface and a smooth transition in the physical properties across the interface. Moreover, the LS approach confines the effect of the volumetric surface force to a narrow region around the interface and this is a vital property for micro-channel condensation simulation due to their small diameter. In many regards the VOF and LS methods provide complementary benefits for the calculation of the free surface flow problem. Therefore, the two methods are coupled in this study. The VOF model is utilised to capture and track the interface location, but enhanced with a LS approach to capture the sharp interface between liquid and vapour. Given the scale of the tubes generated by AM, it is clearly of critical importance that we have a precisely identified location for the interface, and the presence of parasitic currents would represent a major challenge. At the same time, since we are interested in the phase change rate, phase conservation is also of paramount importance. All these factors are dealt with in our combined modelling.

1.2. *Condensation modelling*

As discussed above, CFD is a useful tool to predict flow behaviour in heat exchangers. The current project examines heat exchangers for fuel cells; one of the main functions of which is to condense water out of the exhaust for reuse. Accordingly in this section we will review approaches to modelling condensation.

Some progress has been made in developing and validating numerical models for condensation, but typically this has only involved simple geometries such as rectangular channels. As an example, Ambrosini and collaborators (Ambrosini et al. 2007, 2008, 2014) have performed experiments on a simple rectangular channel and compare it with a 2D model with parallel plates. For the computational part, in addition to several commercial codes, in-house developed codes are used and compared. In other work, De Schepper (Schepper et al. 2009) studied evaporation and condensation phenomena using VOF and a Piecewise Linear Interface Calculation (PLIC) method to reconstruct the two phases between the two phases in every computational cell. The model is used for simulation of the evaporation of hydrocarbon feedstock in the convection section of a steam cracker. Phase change phenomena have also been implemented in steady state conditions (Wang and Rose 2005). This model is based on the Nusselt assumptions but also takes into account the streamwise shear stress on the condensate film surface and the transverse pressure gradient due to surface tension in the presence of curvature of the condensate surface. Further theoretical studies have been performed by the same authors including the effects of surface tension, vapour shear stress and gravity in various cross-sectional channel shapes including square, triangle, inverted triangle, rectangle with longer side vertical, rectangle with longer side horizontal, and circle (Wang and Rose 2006, 2011). More recently, a framework for two-phase flow simulations with thermally driven phase change work has published by Rattner and

Garimella (2014, 2018). Further information and a more complete review of the subject can be found in the recently published review article about computational modelling of boiling and condensation by Kharangate and Mudawar (2017).

The reverse process to condensation is evaporation or boiling, and it is informative to examine the situation here as well, particularly as there has been more concentration on this process in the literature. One of the first experimental investigations of the boiling process measured the effect of heat flux and surface roughness on the wall temperature during the boiling of water (Jakob and Fritz 1931). Over the last decades, measurement and experimental techniques have rapidly improved. Resolved time and length scales have become smaller and smaller and measurement errors have reduced. These have allowed the investigation of local instantaneous quantities, for example wall temperature and heat transfer underneath single vapour bubbles nucleating periodically from a single site (Yaddanapudi and Kim 2001; Demiray and Kim 2004).

At the same time, modelling of boiling heat transfer has been developing rapidly in hand with the growing computing capacities. Again, this requires the simulation of a free surface flow problem which can be accomplished with VOF or Level Set (LS) methods (or others). One significant advantage of the VOF method is its inherent ability to conserve mass in the individual phases, (in the absence of any explicit mass transfer terms in the equations, of course). An early example is the use by Welch and Wilson (2000) of the VOF method to simulate the 1D Stefan test problem. Transient heat conduction with film boiling on a horizontal wall was investigated using similar methods by Welch and Radichi (2005). Shu (2009) combined the advantages of both LS and VOF methods to develop a model of boiling heat transfer which was able to capture the conjugate heat transfer between solid and fluid and the microscale heat transfer at the three phase contact line. However in this case the LS and VOF local coupling was implemented only for structured and orthogonal meshes, which makes the model difficult or almost impossible to use in complex geometries. The boiling heat transfer consists of a meniscus region, evaporating thin film region and a nanoscale non-evaporating region. Several modelling studies have taken into account the effect of those regions to the evaporation process (Wang et al. 2007, 2008). Meanwhile, Hardt and Wondra (2008) examine an evaporation model for interfacial flows which can be implemented into either VOF or LS methods for both film boiling and droplet evaporation.

1.3. *Current work*

The scope of the present work is heat and mass transfer in a condensing heat exchanger. Our simulations rely on VOF methods to represent the bulk liquid phase coupled with LS models to sharpen the interface. The condensation modelling, on the other hand, is based on Ganapathy's work (Ganapathy et al. 2013). These models have been implemented in the open source code OpenFOAM(Weller et al. 1998). In order to examine the capturing of the sharp interface, the Stefan problem (Alexiades and Solomon 1993) is examined and LS-VOF and VOF methods are compared with the analytical solution for this case The complete model is then applied to a series of complex geometries for heat exchanger tubes manufactured using AM, and compared with in-house experiments (performed on AM-manufactured components). The heat exchanger itself is a novel design intended to integrate with a fuel cell for automotive applications, making use of additive manufacture to develop a compact lightweight

unit using complex pipe geometries. This therefore represents the application of novel modelling techniques to a real world test case involving complex geometry, rather than the simplistic geometries investigated previously in the literature. In particular; although other authors have experimented with blending LS and VOF methods for free surfaces, our work represents the first use of this technique for phase change with heat transfer. The main contributions of this work are presented here as the following:

- The combined LS-VOF method is used for the first time for condensation heat transfer modelling on an arbitrary polyhedral mesh.
- To show the improvement of LS-VOF method for the interface (vital for micro channel simulations due to their size), the code is tested by comparison with the analytical solution for the Stefan problem (Alexiades and Solomon 1993).
- The complete condensation model is applied for the first time for complicated industrially related geometries designed for AM.
- A series of in-house experiments and simulations are compared in order to validate the code for real life applications.

The structure of the rest of the paper is as follows. In section 2 we describe the experimental apparatus used for in-house measurement of the condensation. Section 3 details the mathematical models making up the condensation model and describes their implementation in the open source CFD code OpenFOAM. In section 4 we present the validation of the interface modelling (section 4.1) and the application of the whole model to the AM manufactured cases (section 4.2). Finally we summarise the main findings of the work (section 5).

2. Experimental Set-up

In the experiment, we study the counter flow of a heat exchanger consisting of 42 microchannels (see Fig.1) manufactured using AM. The apparatus includes the heat exchanger, 3 reservoirs, pneumatic/hydraulic pump, electric motor, and is instrumented with temperature, flow rate and pressure sensors. There are two circuits; the hot side (saturated air which will be cooled to condense the water vapour) and the cold side, whose function is to provide the cooling. The coolant, a mixture of 50 % glycerol and 50% water, enters and exits at opposite ends of the exchanger. The system is set up as a counterflow heat exchanger with hot side and cold side flowing in opposite directions; in the heat exchanger itself, hot side and cold side microchannels alternate in layers and are fed by complex manifolds. For both circuits, inlet and outlet temperatures and pressures (and therefore temperature changes and pressure drops across the microchannels) are all measured. For the hot side, heated air is pumped through at the desired flow rate. The heated air is passed through a steamer bath to ensure the air humidity reaches the saturation point, and a glass tube is located next to the inlet to divert any liquid water that may have condensed before entering the system, to ensure that only saturated vapour enters the system without any liquid. At the other end, timed collection is used to measure the integrated condensation rate in the system.

The actual test units manufactured using AM are shown in Fig. 3 (front 3 units) and a full 3D CAD model is shown in Fig.2. As shown in Fig.2 the blue coolant side has 2 inlets and 2 outlets and the red coloured microchannels, supplied by a separate manifold (not shown) are the condensing part of the heat exchanger. A number of different micro-geometries were investigated; of which 3 are presented here. These are a. straight micro-channels of constant diameter as a base-line case, b. the same constant

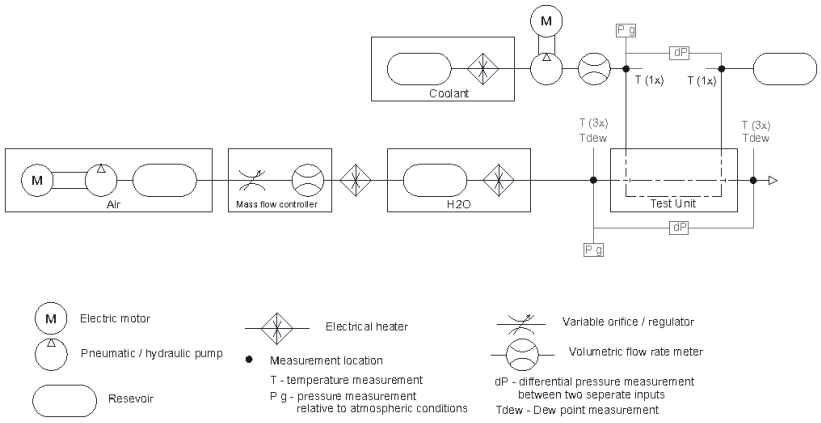

Figure 1. Experimental set-up scheme.

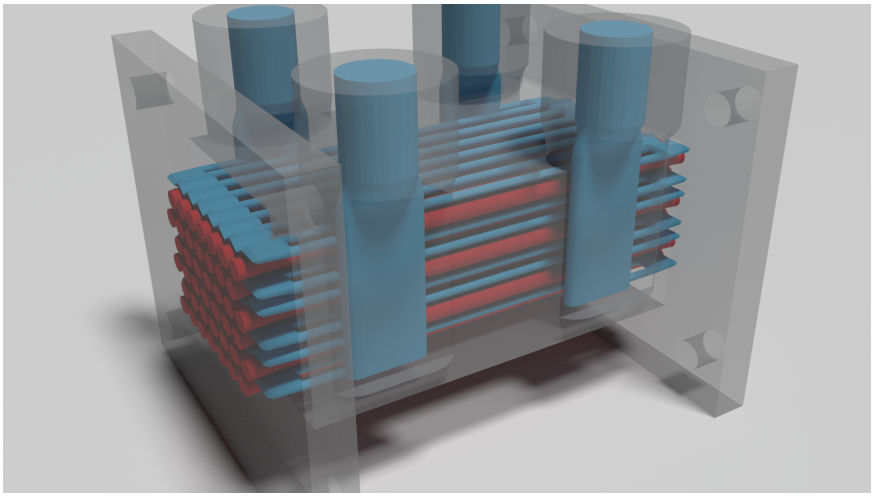

Figure 2. Full test unit with straight micro-channels.

cross-sectional microchannel twisted into a helix around the streamwise direction, and c. this helical geometry augmented with a sinusoidally varying diameter. These are referred to as straight, helical and helical expanded geometries respectively.

3. Numerical Modelling

The physical processes involved in the heat exchanger are complex and include phase change and heat transfer. Figure 4 provides a schematic cross-section to clarify the details of the modelling; the different physical aspects of which are explained below.

3.1. *Governing Equations*

In interface-capturing methods such as VOF and LS, a single set of the Navier-Stokes equations is shared by the participating fluids. Since the flow here is laminar ($\mathcal{R}e =$

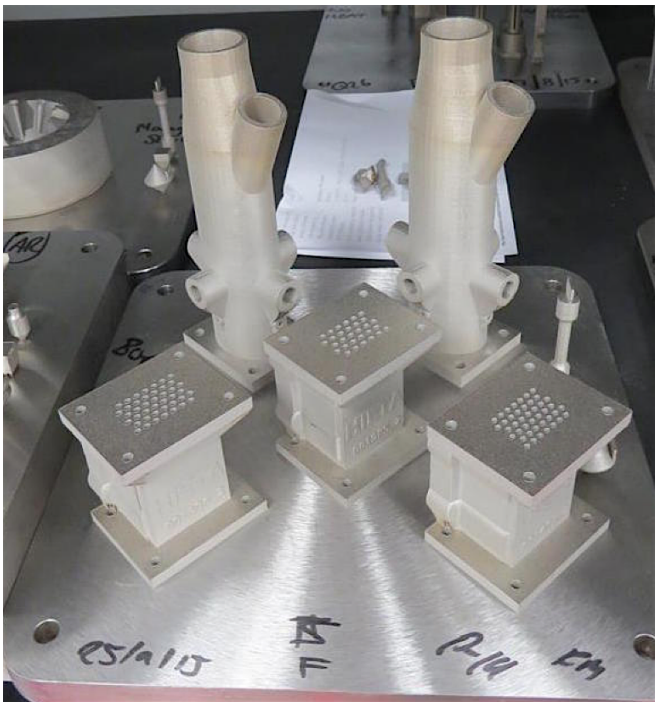

Figure 3. Test units.

950), the continuity equation for the mixture is given in Eq.1:

$$\frac{\partial \rho_m}{\partial t} + \nabla \cdot \left(\rho_m \vec{U} \right) = 0 \tag{1}$$

whilst Eq.2 represents the momentum equation:

$$\frac{\partial \rho_m \vec{U}}{\partial t} + \nabla \cdot \left(\rho_m \vec{U} \vec{U} \right) = -\nabla p + \nabla \cdot \left(\mu_{eff} \nabla \vec{U} \right) + \vec{F}_\delta \tag{2}$$

On the left hand side (LHS), the first term represents the unsteady term, the second term describes the convective term. On the right hand side (RHS), the first term represents the pressure gradient, the second term describes diffusion and last one represents the external forces.

The conservation of energy equation is written as Eq.3:

$$\frac{\partial \rho_m C_{p,m} T}{\partial t} + \nabla \cdot \left(\rho_m \vec{U} C_{p,m} T \right) = \nabla \cdot (\lambda \nabla T) + S_h \tag{3}$$

where mixture properties are calculated as follows

$$\rho_m = \rho_l (1 - \alpha) + \alpha \rho_v \tag{4}$$

$$C_{p_m} = C_{p_l} (1 - \alpha) + \alpha C_{p_v} \tag{5}$$

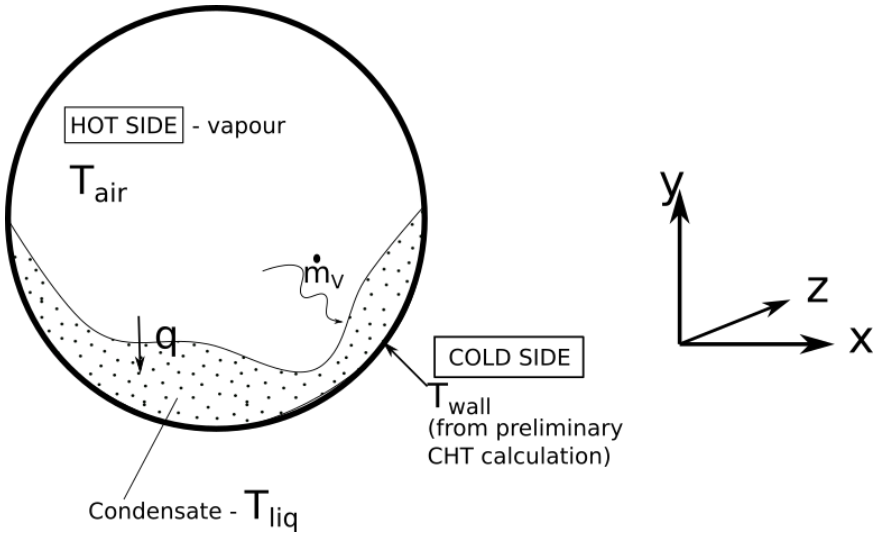

Figure 4. Schematic indicating the geometry and physical processes occurring in the simulation. $\dot{m}_v$ is the mass transfer between phases due to condensation and q the heat flux between the phases.

$$\lambda_m = \lambda_l(1-\alpha) + \alpha\lambda_v \tag{6}$$

where $C_{p,m}$ is the specific heat capacity and λ the coefficient of thermal conductivity. On the LHS the first term is the temperature change over time and the second term is the temperature convection term. On the RHS the first term is the temperature diffusion and the last term is the temperature change due to condensation.

The VOF approach needs additionally to solve an equation for an indicator function α, as follows

$$\frac{\partial\alpha}{\partial t} + \nabla\cdot\left(\alpha\vec{U}\right) + \nabla\cdot\left(\vec{U}_c\alpha(1-\alpha)\right) = S_e - S_c \tag{7}$$

where S_c and S_e denote the rate of mass transfer for condensation and evaporation, respectively. The last term on the LHS represents an artificial compression term introduced to sharpen the interface. This term has a non-zero value only at the interface due to the $(\alpha(1-\alpha))$ term. U_c is the appropriate velocity field to describe the interface compression. This artificial compression determines the smoothness of the interface between each of the phases; it does not affect the solution but only defines the flow of α in the normal direction to the interface.

$$U_c = min\left[C_\alpha|\vec{U}|, max(|\vec{U}|)\right]\frac{\nabla\alpha}{|\nabla\alpha|} \tag{8}$$

Eq.8 describes the compression velocity dependent on the maximum value at the interface. U_c can be controlled by a term C_α which limits the artificial compression velocity. If there is no compression then $C_\alpha = 0$, whilst if $C_\alpha = 1$ there is conservative compression. The last option is $C_\alpha > 1$ which means there is high compression. In a conventional VOF model, the indicator function would be used to blend physical prop-

erties of the constituent fluids in the system; however here we are using LS methods to sharpen the interface and so these will be used to compute the mixture properties as detailed in section 3.2.

3.2. *Level Set and Volume of Fluid formulation*

The first step in blending the LS (Albadawi et al. 2013; Sussman and Puckett 2000; Osher and Fedkiw 2001) and VOF methods is the initialisation of the value for the LS function from the VOF indicator function field α

$$\phi_0 = (2\alpha - 1)\,\Gamma \tag{9}$$

where $\Gamma = 0.75\Delta x$ and Δx is a characteristic cell size in the region of the interface. The initial value describes the signed distance function, taking negative values for gas and positive values for liquid. The following re-initialisation equation is solved in order to calculate the new distance ϕ to the interface in the LS

$$\frac{\partial \phi}{\partial \tau} = S\left(\phi_0\right)\left(1 - \nabla\phi\right) \tag{10}$$

$$\phi\left(x, 0\right) = \phi\left(x\right) \tag{11}$$

where τ is an artificial dimensionless time variable which is defined as $0.1\Delta x$. The solution converges to $|\Delta\phi| = 1$. $S(\phi_0)$ is a signum function which can be defined as follows

$$S(\phi_0) = \begin{cases} -1 & if \quad \phi < 0 \\ 0 & if \quad \phi = 0 \\ 1 & if \quad \phi > 0 \end{cases} \tag{12}$$

The iteration number is calculated by $\phi = \epsilon/\Delta\tau$ where the interface thickness is calculated by $\epsilon = 1.5\Delta x$. From this the surface can be calculated as

$$\vec{F}_\delta = \sigma\kappa\left(\phi\right)\delta\left(\phi\right)\Delta\left(\phi\right) \tag{13}$$

where σ is a surface tension coefficient, $\kappa\left(\phi\right)$ is the curvature a and the middle term δ is the Dirac function which limits the influence of the surface tension within the interface. For numerical reasons the Dirac function is represented by the C^1-continuous function

$$\delta(\phi) = \begin{cases} 0 & if \quad |\phi| > \epsilon \\ \frac{1}{2\epsilon}\left[1 + cos\left(\frac{\pi\phi}{\epsilon}\right)\right] & if \quad |\phi| \leq \epsilon \end{cases} \tag{14}$$

The integral of this is the Heaviside function which can thus be used as the indicator function to distinguish between the two fluids making up the system. Again this is approximated by the C^1-continuous function

$$H(\phi) = \begin{cases} 0 & if \quad \phi < -\epsilon \\ \frac{1}{2}\left[1 + \frac{\phi}{\epsilon} + \frac{1}{\pi} sin\left(\frac{\pi\phi}{\epsilon}\right)\right] & if \quad |\phi| \geq \epsilon \\ 1 & if \quad \phi > \epsilon \end{cases} \tag{15}$$

and the mixture properties can be represented in terms of this as

$$\rho_m = H\rho_l + (1 - H)\,\rho_g \tag{16}$$

$$\mu_{eff} = H\mu_l + (1 - H)\,\mu_g \tag{17}$$

where l is the liquid and g is the gas phase.

3.3. *Phase change*

The phase change modelling methodology is based on the work of Ganapathy et al. (2013). This model avoids the use of case-specific constant parameters or experimental correlations and is therefore appropriate to simulate any kind of flow regime. The VOF-LS interface capturing method includes terms S_c and S_e representing transfer between the phases due to condensation and evaporation respectively. In the current case, only condensation is being considered. In addition the latent heat of condensation must be included as the source term S_h in Eq.3 in order to describe phase change. Fourier's law is used for estimation of the heat flux q associated with phase change in Eq.18 and relates to the condensation mass flux $\dot{m}_l$ and latent heat of condensation h_{LV}.

$$q = -\lambda_m \times (\nabla T) = \dot{m}_v \times h_{LV} \tag{18}$$

Condensation takes place at the interface, which can be identified by multiplying by $\nabla\alpha$, so

$$S_c = \frac{q \cdot \nabla\alpha}{h_{LV}\rho_m} \tag{19}$$

Based on this, the energy source term is

$$S_h = S_c \times h_{LV} \times \rho_m \tag{20}$$

The rate of mass transfer from vapour to liquid is given by

$$\dot{m}_v = \frac{\lambda_m\,(\nabla\alpha \cdot \nabla T)}{h_{LV}} \tag{21}$$

3.4. *Numerical aspects and Meshing*

The above equations are implemented in the open source Computational Continuum Mechanics library OpenFOAM, with existing codes within the distribution being modified to introduce the novel computational modelling. The PIMPLE algorithmHolzmann (2017) (blended PISO/SIMPLE, implemented as `pimpleFoam`) was

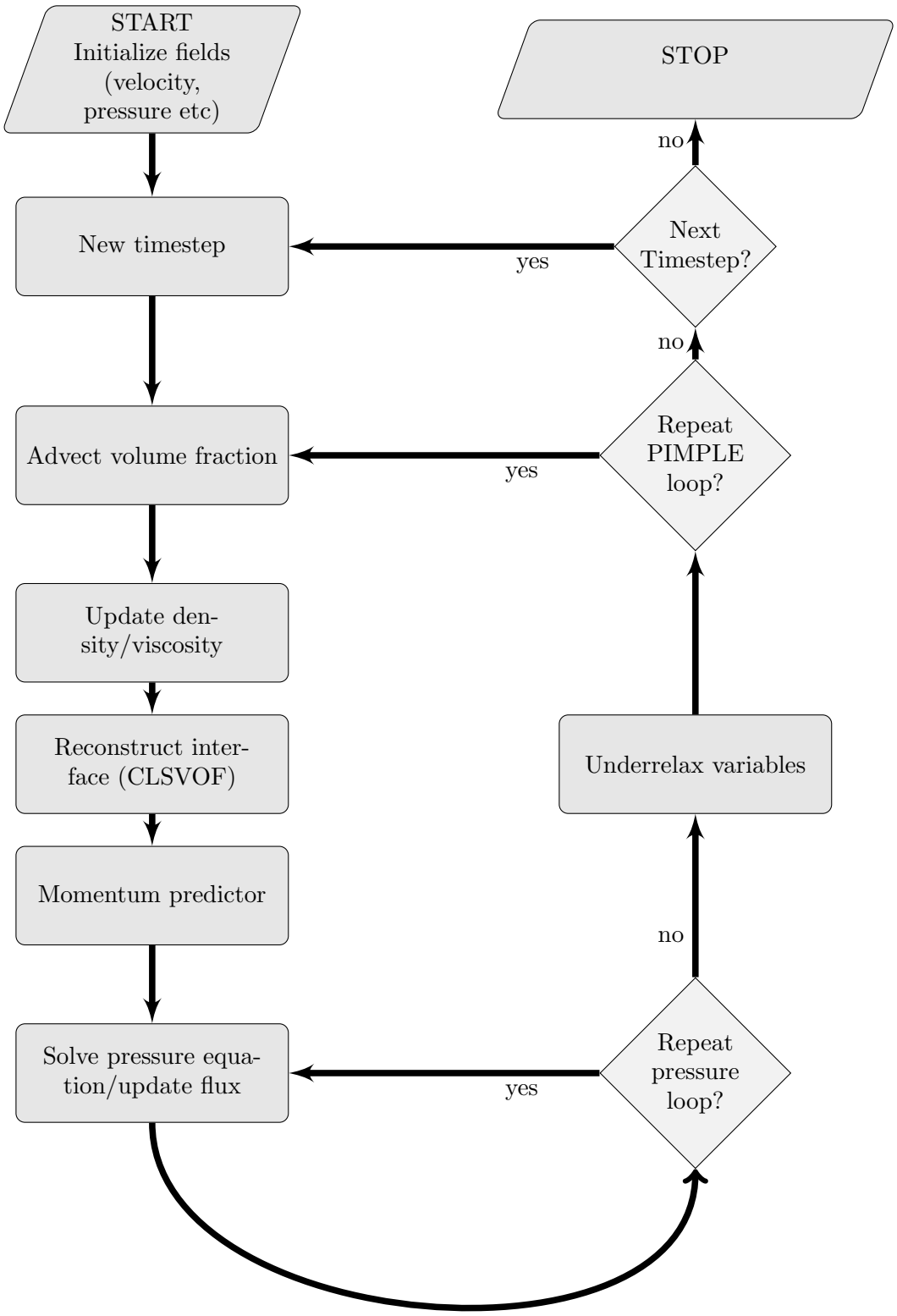

Figure 5. Flow chart showing the integration of the modelling into the PIMPLE loop.

used to solve the equation set as a segregated solve. The sequential solution is shown in the flow chart (figure 5) which indicates how the additional modelling has been incorporated into the PIMPLE algorithm. PIMPLE is a timestepping algorithm developed for stability, with an outer loop (the PIMPLE loop) including underrelaxation of the variables, and an inner pressure correction loop (based on the PISO algorithm). The new modelling representing the interface modelling is evaluated within the PIMPLE loop before the momentum predictor step in order to provide updated values for the mixture density and viscosity at this point, so these values are evaluated each pass through the outer PIMPLE loop. Second order numerics have been used throughout. For time discretisation, the Euler method has been used Lee (2017); divergence terms in the momentum equation are discretised using a 2nd order upwind scheme, and divergence terms in the α equation are discretised using the van Leer scheme.

OpenFOAM is based on the Finite Volume method, in which the domains of interest are split into numerous individual control volumes or cells within a mesh. Meshing of the complex domains of interest was quite challenging, and was accomplished using the separate meshing code Pointwise. Because of the complexity of performing a fully coupled simulation of both the hot and cold sides of the heat exchanger together with the phase change modelling, the decision was made to model the phase change behaviour separately. A preliminary calculation was therefore performed on the heat exchanger using an existing conjugate heat transfer (CHT) solver in OpenFOAM (chtMultiRegionSimpleFoam) in order to define the temperature boundary conditions for the main calculations of heat transfer and condensation in the hot side using the modelling described above. The set up for the CHT calculation is shown in Table 1. Stainless steel is used as a material and wall thickness between the channels was approx. 2 mm.

Flow domain	Boundary conditions
Hot side	$\dot{m}$ 0.0447 kg/s
	T 366.85K
Cold side	$\dot{m}$ 0.43 kg/s
	T 323.15 K

Table 1. Boundary conditions for the CHT simulation

On the hot side simulation, a variety of meshes with resolutions from 91k to 1.3 million cells were generated and computed to understand the mesh sensitivity. Results were essentially identical for the two largest meshes of 900,000 and 1.3 million cells, indicating a good degree of mesh independence of the results. To illustrate this, figure 6 shows condensation rates calculated for one of the geometries (helical expanded channel; selected as one of the more complex geometries) on three meshes with cell counts of 91200 cells (black), 631150 cells (blue) and 912220 cells (red). All 6 cases given in Table 2 are shown (cases case1 – case6). This shows no significant dependency of condensation rate on cell count. The results presented in the rest of the paper are for the 1.3 million cell case as this was felt to have better near-wall resolution.

4. Results

In this section we present results from two independent calculations. In subsection 4.1 we present comparison with the well known one dimensional Stefan problem (see Fig. 2) for which the interface position can be calculated analytically; this enables us to compare the behavior of the interface capturing using simple VOF and our advanced

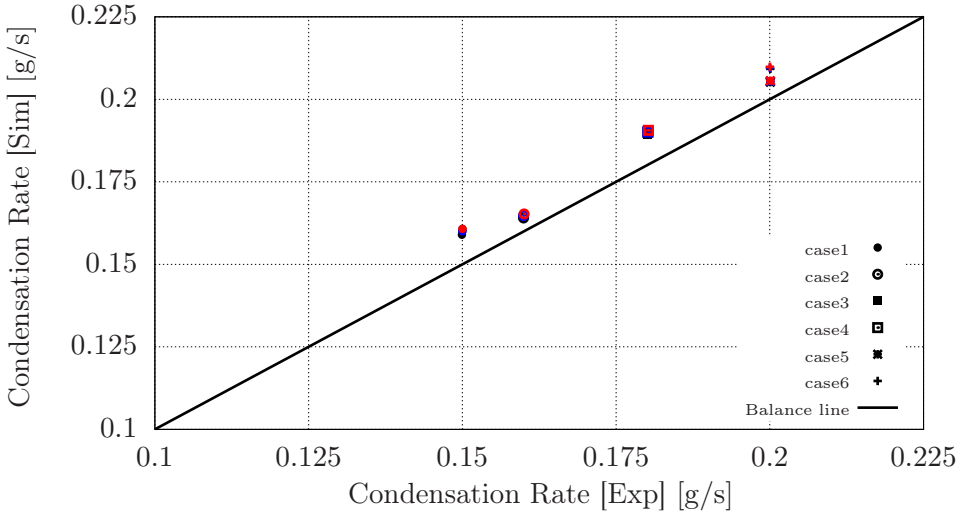

Figure 6. Mesh sensitivity results for condensation rate for a helical expanded microchannel. Results are shown for meshes of 91200 cells (black), 631150 cells (blue) and 912220 cells (red) for the 6 different flow rates shown in table 2.

LS-VOF formulations. In the second subsection simulations and experimental results are presented for 3D geometries for AM heat exchangers designed for fuel cell applications. A number of different micro-geometries were investigated; of which 3 are presented here. These are a. straight micro-channels of constant diameter as a base-line case, b. the same constant cross-sectional microchannel twisted into a helix around the streamwise direction, and c. this helical geometry augmented with a sinusoidally varying diameter. These are referred to as straight, helical and helical expanded geometries respectively. The different mass flow rates are shown in the table 2.

4.1. *1D Stefan problem*

In order to demonstrate the improvement in interface capturing using the LS-VOF method over the VOF method, solutions using both methods are compared with the analytical solution for the one dimensional Stefan problem (Alexiades and Solomon 1993). In general, Stefan problems describe 1d phase change problems in which the location of the phase interface has to be modelled. In this case, as shown in figure 7, the problem concerns the conversion of liquid to superheated vapour near a heated wall, where the wall temperature is higher than saturated temperature. The vapour is heating up and becoming superheated near the wall, whilst mass transfer take place at the interface.

The exact location of the interface as a function of time can be calculated from the following analytical equation:

$$\delta(t) = 2\varepsilon\sqrt{\frac{\lambda_V t}{\rho_v C_{P,V}}} \tag{22}$$

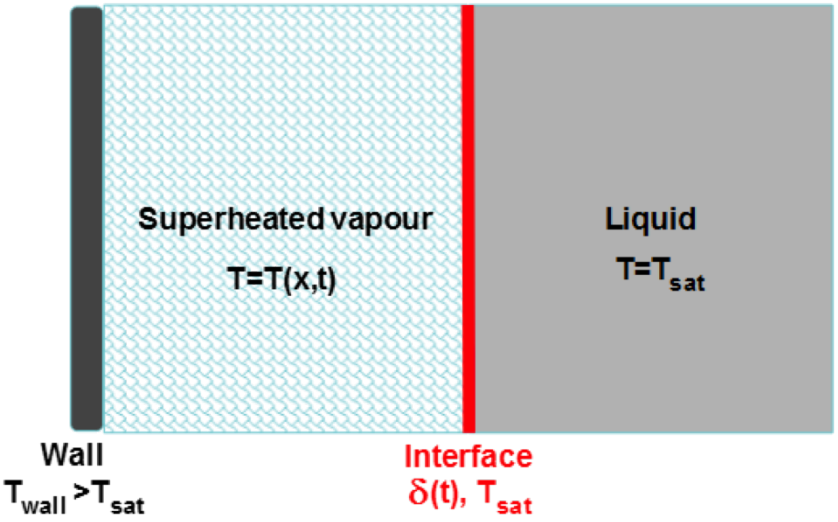

Figure 7. Schematic diagram of one-dimensional Stefan problem.

where ε can be calculated from the following implicit equation,

$$\varepsilon \, exp(\varepsilon^2) \, erf(\varepsilon) = \frac{C_{P,V}(T_w - T_{sat})}{h_{LV}\sqrt{\pi}} \tag{23}$$

where thermal conductivity λ_V=0.005 W/m K, specific heat $C_{P,V}$= 200 J/kg K,

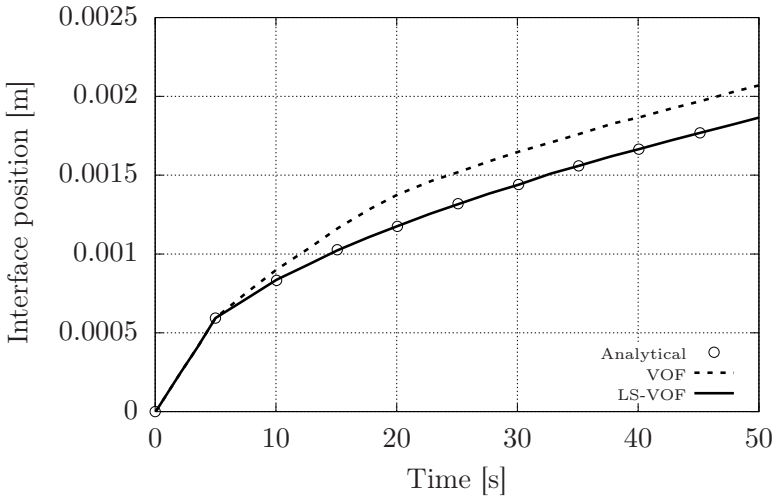

Figure 8. Interface position respect to the time with LS-VOF, VOF and analytical solution

saturated liquid ρ_v=1kg/m^3 density and latent heat h_{LV}=10^4 J/kg. The difference between the saturated temperature and the wall temperature is 10 K.

The results as shown in Fig. 8 demonstrate that the LS-VOF method predicts the interface location very accurately whereas VOF is $10-15\%$ off from exact solution. This is due to the the interface location being smeared across several cells; even with a very fine resolution mesh, the exact position of the interface is not well defined. In

addition, parasitic currents in the VOF method would cause substantial problems with the modelling of flow in the AM microchannels. Our new LS-VOF method effectively resolves both these problems.

4.2. *Real 3D case simulations and validation*

Test cases for straight micro channels					
Case Name	Vapour Mass Flow Rate [g/s]	Inlet Temperature [°C]	Condensation Rate (Exp)[g/s]	Condensation Rate (Sim)[g/s]	Deviation [%]
case 1	0.187	94.63	0.12	0.129	2.0
case 2	0.185	94.47	0.12	0.127	1.4
case 3	0.191	93.36	0.13	0.135	1.3
case 4	0.228	94.17	0.13	0.136	1.7
case 5	0.234	94.59	0.13	0.139	1.7
case 6	0.248	93.75	0.13	0.141	1.4
Test cases for helical microchannels					
Case Name	Vapour Mass Flow Rate [g/s]	Inlet Temperature [°C]	Condensation Rate (Exp)[g/s]	Condensation Rate (Sim)[g/s]	Deviation [%]
case 1	0.181	93.80	0.15	0.159	1.5
case 2	0.186	93.22	0.16	0.164	2.5
case 3	0.222	93.74	0.18	0.189	1.0
case 4	0.235	92.84	0.18	0.189	1.0
case 5	0.263	92.94	0.20	0.205	2.4
case 6	0.252	93.98	0.20	0.209	3.0
Test cases for helical expanded microchannels					
Case Name	Vapour Mass Flow Rate [g/s]	Inlet Temperature [°C]	Condensation Rate (Exp)[g/s]	Condensation Rate (Sim)[g/s]	Deviation [%]
case 1	0.187	94.21	0.16	0.165	1.6
case 2	0.185	93.92	0.17	0.179	1.1
case 3	0.191	93.62	0.18	0.187	0.7
case 4	0.228	93.57	0.20	0.205	2.0
case 5	0.234	93.61	0.21	0.216	2.0
case 6	0.248	93.69	0.21	0.211	0.5

Table 2. Comparison of integrated condensation rates from experiment and simulation for straight, helical and helical expanded cases. Estimated experimental errors are $\sim 5\%$. Deviation is the % discrepancy between experimental and computational results, which is well within experimental error.

Having demonstrated the efficacy of the new LS-VOF method, we now compare results for the full condensation model against our in-house experimental results for the three different microchannel geometries. Initially the overall integrated condensation rates, together with pressure and temperature differences between inlet and outlet, are compared with the experimental data. During the experiment, the total condensation rate was measured by timed collection. In the simulation the condensation rate is calculated in terms of the source term S_c which is an intensive variable, and so this

has to be integrated over the domain to determine the calculated condensation rate;

$$CondensationRate = \int_V S_{\alpha_i}\, dx\, dy\, dz \tag{24}$$

As can be seen in Figs. 9, 10 and 11, simulations and experimental data are in excellent agreement for all cases. The numerical values are also given in table 2, and show a maximum error of 3%; Case 2 is not included in Fig. 9 because it was very similar to Case 1.

Overall pressure differences between inlet and outlet are given in table 3. For the straight microchannel case – laminar flow in a straight pipe with constant circular cross-section – there is of course a straightforward analytical solution, and this has been calculated for comparison; giving a 1.5% error for the respective computational solution.The more complicated geometries of the helical and helical expanded cases increase the surface area of the microchannel and thus increase the frictional losses, leading to higher pressure drops. The same increase in surface area of course also enhances heat transfer, and there is an obvious tradeoff between the two parameters of the system. The exact details of how the geometry affects the pressure drop is examined in Fig. 12, which shows the variation in pressure in the flow direction along the channels for the helical and helical expanded cases and core part of the simulation domain. The change of diameter along the helical expanded geometry case is reflected in the oscillatory pressure profile, whilst in the helical case the diameter stays the same even though the microchannel is curved overall. It can be seen from Fig.12 that the expanded helical geometry has more than twice the pressure loss compared to the helical case. The comparison has also been performed for helical and helical expanded cases with experimental data for the temperature difference between inlet and outlet, and the results are in good agreement as can be seen in Table 4; the maximum discrepancy here being 0.2%.

Channel Type	Pressure Drop [Pa]
Analytical solution	90.45
Straight	91.8
Helical	174
Helical expanded	515

Table 3. Table of pressure drops for straight, helical and helical expanded cases

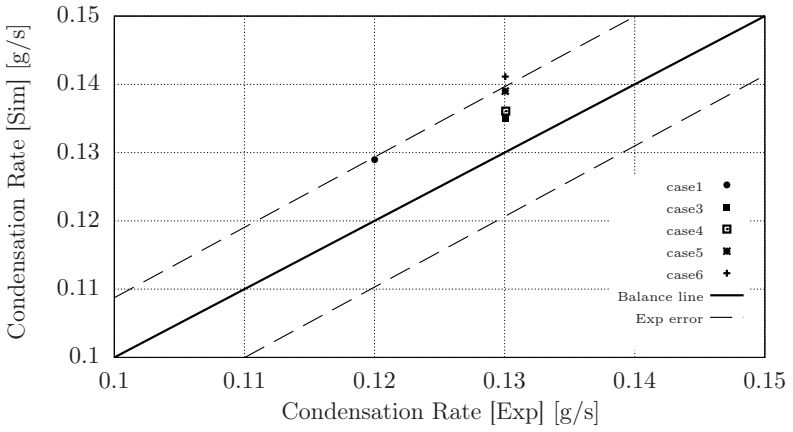

Figure 9. Condensation rate in straight microchannel for various flow rates.

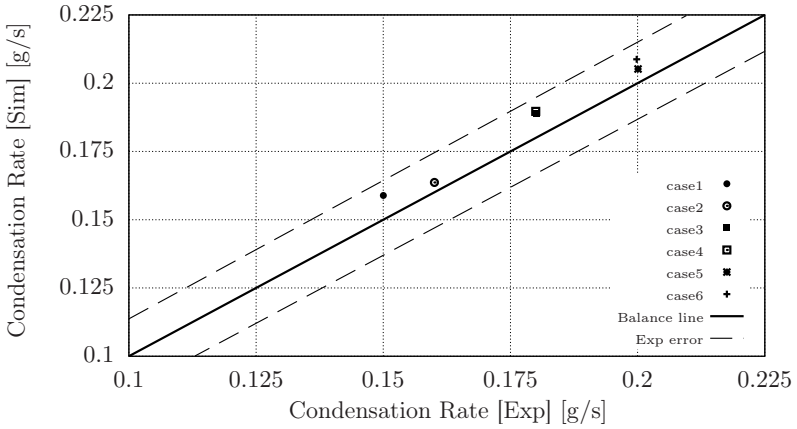

Figure 10. Condensation rate in helical microchannel for various flow rates.

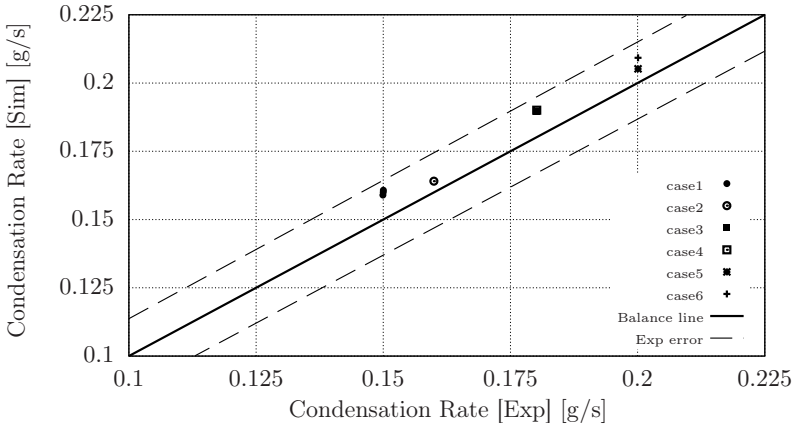

Figure 11. Condensation rate in helical expanded micro-channel for various flow rates.

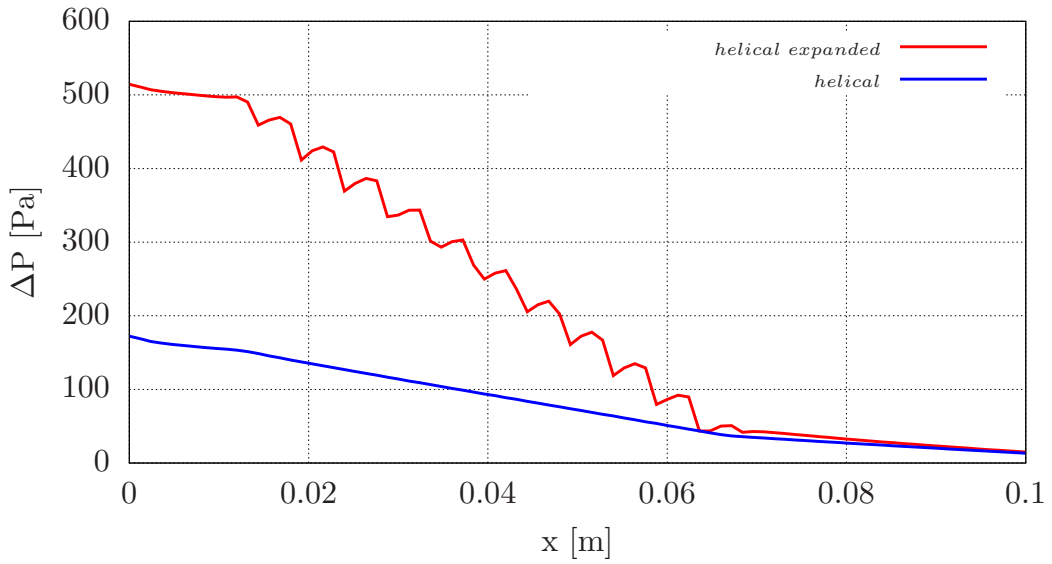

Figure 12. Pressure drop comparison of simulation for the helical expanding(dots) and helical(square) microchannels.

Channel Type	Temperature Difference [K]	
Helical	Sim	26.88
	Exp	26.85
Helical expanded	Sim	26.74
	Exp	26.68

Table 4. Temperature difference at inlet/outlet helical expanded and helical microchannel

Fig. 15 shows profiles of the localised condensation rate at three locations along the heat exchanger. As expected the condensation mid channel is essentially zero for all cases; condensation occurs at the outer edges near the walls where the heat transfer rate and therefore cooling is greatest. A significant increase in the condensation rate can be seen in the last part ($x/D = 20$) of Fig. 15 in the helical expanded geometry due to its better cooling abilities, as seen in Fig. 13. Fig. 13 also shows colour plots for the helical and helical expanded cases, showing how temperature, condensation rate and water volume fraction change downstream along the microchannel. The enhanced heat exchange and thus condensation rate is not merely a function of the increased surface area of these designs over the simple straight microchannel, but as has been observed elsewhere (Turnow et al. 2011), the complex geometry of the helix provides the possibility of regions of stagnation or recirculation which help to extract the energy from the main flow and thus enhance the cooling process. The presence of these stagnation regions can be seen in figure 14 which shows a detailed view of the helical geometry using both streamlines and colour plots to visualise the flow. This is taken even further in the helical expanded geometry as the expansion sections of the microchannel result in further slowing of the flow. Fairly obviously from the condensation rate and water volume fraction plots, the water accumulates preferentially in these regions and builds into a laminar film near the wall as expected and explained in the literature (Collier and Thome 1996). Moreover, the solver predicts the water layer to grow downstream along the micro-channel walls as would be expected.

5. Conclusions

A complete model for simulating condensation in a heat exchanger has been developed and implemented within the OpenFOAM framework. The model comprises two parts; a LS-VOF model for interface tracking to identify and track the condensate, and a full condensation model to deal with the phase change. The LS-VOF model, implemented for the first time in this context, was validated against the known analytical solution for the 1d Stefan problem and shown to significantly out-perform standard VOF modelling. The sharper interface tracking is vital in simulation of micro-channels and condensation. The condensation model, based on that of Ganapathy et al. (2013), was further developed to include temperature-dependent material properties, and solved together with the heat equation to close the system of equations. Results for condensation rate, pressure and temperature changes across the system have been validated against in-house experimental data on complex geometries manufactured using AM, whilst detailed aspects of the localised condensation and spatial distribution of condensation have been shown to agree with expectation and other work in the area. Direct coupling of the cold and hot flow simulations would be an obvious next step; however the accuracy of the uncoupled condensation simulations, in comparison with the experimental data, suggests that this may not in fact be necessary.

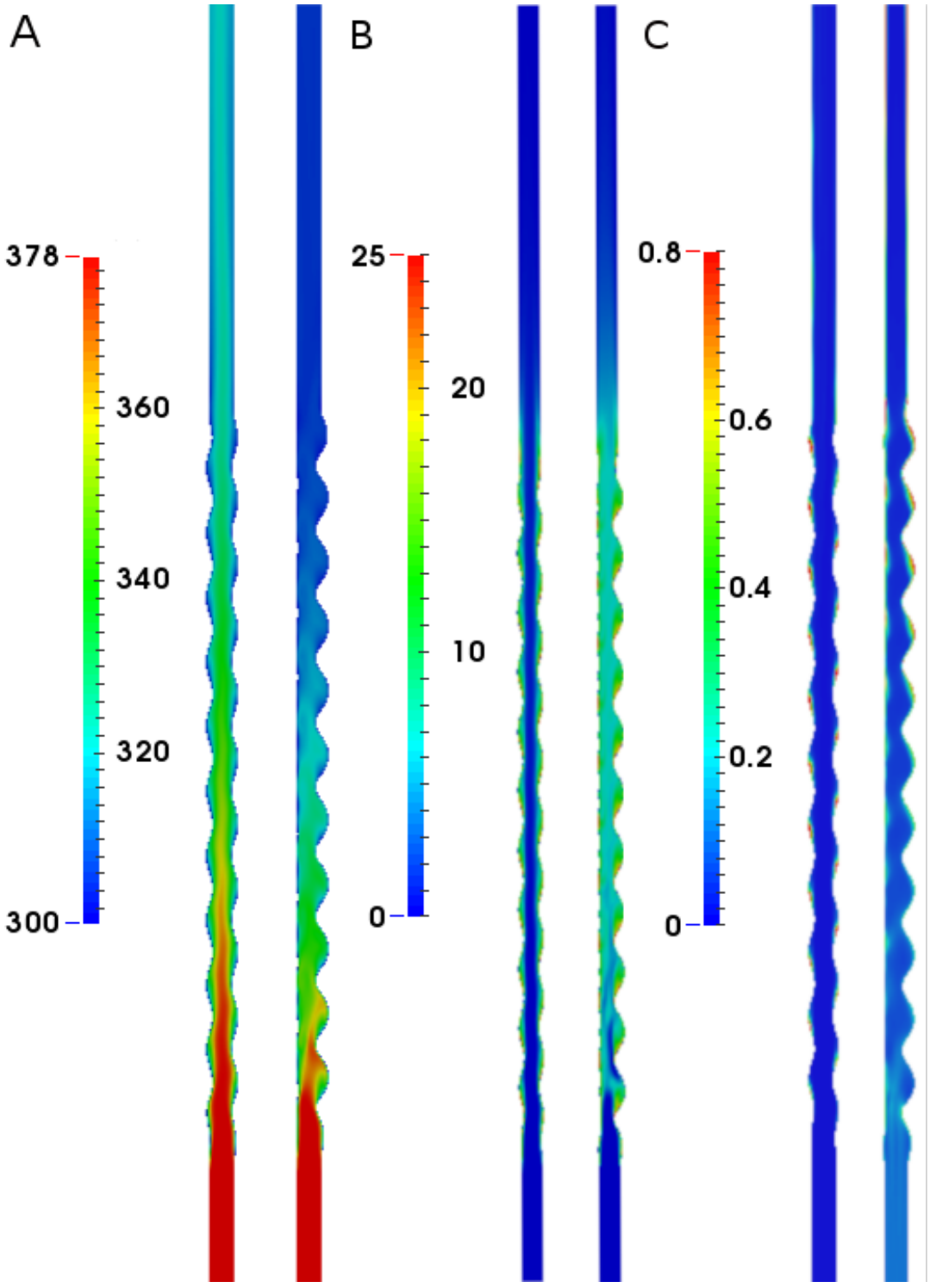

Figure 13. A) Mean values of temperature [K], on cross sections in RHS Helical and LHS Helical Expanded. B) condensation rate [kg/m^3s], on cross sections in RHS Helical and LHS Helical Expanded and C) water volume fraction, on cross sections in RHS Helical and LHS Helical Expanded

References

Albadawi, A., Donoghue, D., Robinson, A., Murray, D., and Delauré, Y. (2013). A coupled level set and volume-of-fluid method for computing 3d and axisymmetric incompressible

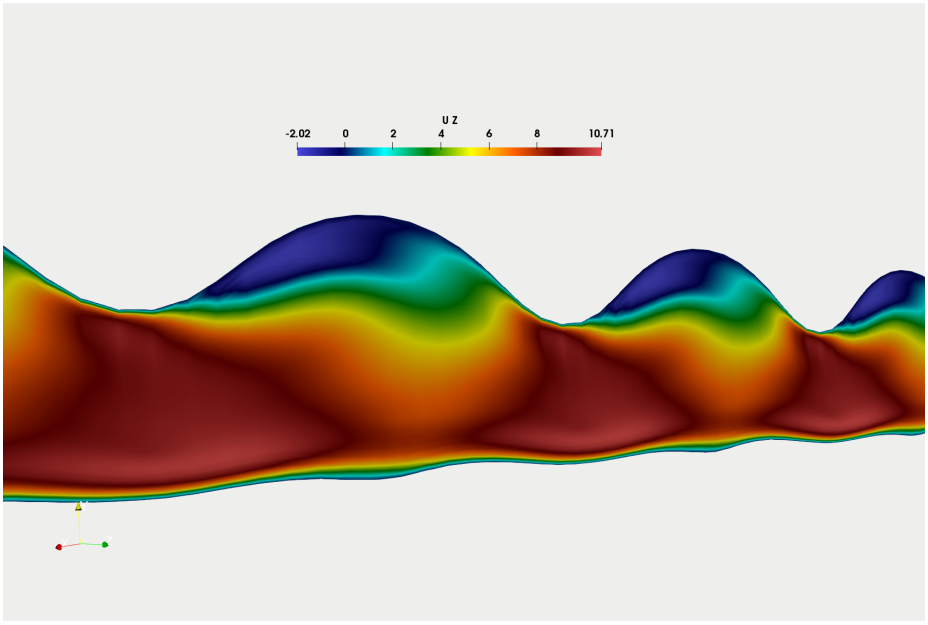

Figure 14. Localised flow in the helical geometry, visualised on a cutting plane down the centre of the duct, showing the stagnation regions created by the complex geometry.

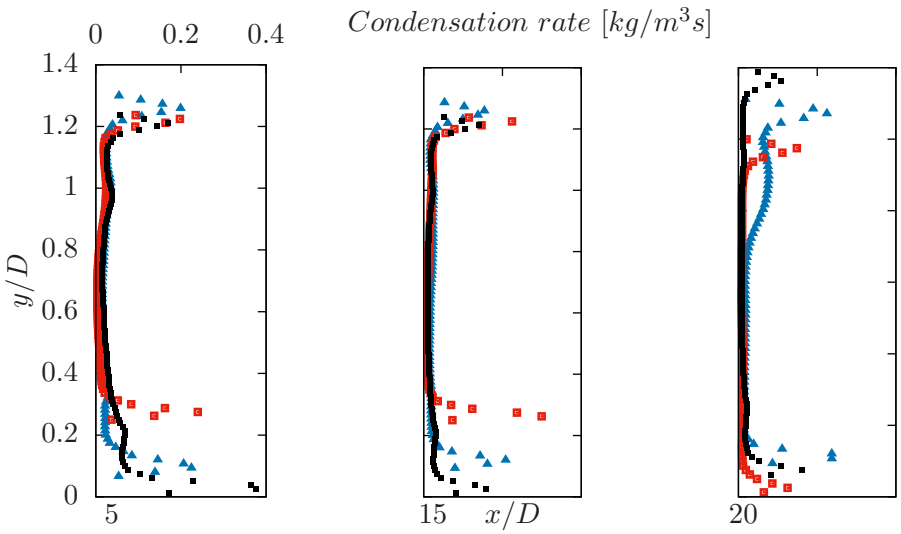

Figure 15. Condensation rate in three different places in the micro-channel for three different geometries: Blue triangle-Helical expanded micro-channel, red square-helical micro-channel, black dots-expanded micro-channel.

two-phase flows. *Int. J. of Multiphase Flow*, 53:11–28.

Alexiades, V. and Solomon, A. (1993). Mathematical modelling of melting and freezing processes. Hamisphere, Washington, DC.

Ambrosini, W., Bucci, M., N.Forgione, Oriolo, F., S.Pacci, and M.Ohadi (2007). Results for the SARnet condensation benchmark no: 0. Dipartimento di Ingegneria Meccanica, Nucleare e della Produzione (DIMNP)006, Universitá di Pisa, Pisa, Italy.

Ambrosini, W., Forgionea, N., Merli, F., Oriolo, F., Paci, S., Kljenak, I., Kostka, P., Vyskocil, L., Travis, J., Lehmkuhl, J., Kelm, S., Ching, Y.-S., and Bucci, M. (2014). Lesson learned from the SARNET wall condensation benchmarks. *Annals of Nuclear Energy*, 74:153–164.

Ambrosini, W., Forgionea, N., Orioloa, F., Paci, S., Magnaud, J.-P., Studer, E., Reinecke, E.,

Kelm, S., W. Jahn, J. T., Wilkening, H., Heitsch, M., Klje-nak, I., Babic, M., M, H., Visser, D., Vyskocil, L., Kostka, P., and Huhtanen, R. (2008). Comparison and analysis of the condensation benchmark results. The 3rd European Review Meeting on Severe Accident Research (ERMSAR-2008), Nesseber, Bulgaria.

Anderson, J. D. (1982). *Time-Dependent Multi-Material Flow with Large Fluid Distortion Numerical Method for Fluid Dynamics.* Academic Press, New York.

Brackbill, J., Kothe, D., and Zemach, C. (1992). A continuum method for modeling surface tension. *Journal of Computational Physics*, 100:335–354.

Collier, J. G. and Thome, J. R. (1996). *Convective Boiling and Condensation.* Oxford University Press, New York.

Demiray, F. and Kim, J. (2004). Microscale heat transfer measurements during pool boiling of FC-72: Effect of subcooling. *Int. J. Heat Mass Transfer*, 47:3257–3268.

Ganapathy, H., Shooshtari, A., Choo, K., Dessiatoun, S., Alshehhi, M., and Ohadi, M. (2013). Volume of fluid-based numerical modeling of condensation heat transfer and fluid flow characteristics in microchannels. *Int.J.Heat Mass Transfer*, 65:62–22.

Hardt, S. and Wondra, F. (2008). Evaporation model for interfacial flows based on a continuum-field representation of the source terms. *Journal of Computational Physics*, 227:5871–5895.

Harvie, D., Davidson, M., and Rudman, M. (2006). An analysis of parasitic current generation in Volume of Fluid simulations. *Applied Mathematical Modelling*, 30(10):1056 – 1066.

Hirt, C. W. and Nichols, B. (1981). Volume of fluid (VOF) method for the dynamics of free boundary. *Journal of Computational Physics*, 39:201–225.

Holzmann, T. (2017). *Mathematics, Numerics, Derivations and OpenFOAM(R).* Holzmann CFD, Leoben, 4th edition edition.

Jakob, M. and Fritz, W. (1931). Versuche ber den Verdampfungsvorgang. *Forschung auf dem Gebiet der Ingenieurwissenschaften*, 2:435–447.

Kharangate, C. and Mudawar, I. (2017). Review of computational studies on boiling and condensation. *Int.J.Heat Mass Transfer*, 108:1164–1196.

Lee, S. B. (2017). A study on temporal accuracy of OpenFOAM. *Int.J. Naval Architecture and Ocean Engineering*, 9:429 – 438.

Osher, S. and Fedkiw, R. P. (2001). Level set methods: An overview and some recent results. *Journal of Computational Physics*, 169:463–502.

Osher, S. and Sethian, J. A. (1988). Fronts propagating with curvature-dependent speed: Algorithms based on hamilton-jacobi formulations. *Journal of Computational Physics*, 79(1):12 – 49.

Rattner, A. and Garimella, S. (2014). Simple mechanistically consistent formulation for volume-of-fluid based computations of condensing flows. *J. Heat Transfer*, 136.

Rattner, A. and Garimella, S. (2018). Simulation of taylor flow evaporation for bubble-pump applications. *J. Heat Transfer*, 16:231–247.

Rusche, H. (2002). *Computational Fluid Dynamics of Dispersed Two-Phase Flows at High Phase Fraction.* PhD thesis, Imperial College of Science.

Schepper, S. D., G.J.Heynderickx, and G.B.Marin (2009). Modeling the evaporation of a hydrocarbon feedstock in the convection section of a steam cracker. *Computers and Chemical Engineering*, 33:122–132.

Shu, B. (2009). *Numerische Simulation des Blasensiedens mit Volume-Of-Fluid-und Level-Set-Methode.* PhD thesis, Technische Universitat Darmstadt.

Sussman, M. and Puckett, E. G. (2000). A coupled level set and volume-of-fluid method for computing 3d and axisymmetric incompressible two-phase flows. *Journal of Computational Physics*, 162:301–337.

Sussman, M., Smereka, P., and Osher, S. (1994). A level set approach for computing solutions to incompressible two-phase flow. *Journal of Computational Physics*, 114(1):146–159.

Turnow, J., Kornev, N., Isaev, S., and Hassel, E. (2011). Vortex mechanism of heat transfer enhancement in a channel with spherical and oval dimples. *Int.J.Heat Mass Transfer*, 47:301–313.

Ubbink, O. and Issa, R. (1999). A method for capturing sharp fluid interfaces on arbitrary

meshes. *Journal of Computational Physics*, 153:26–50.

Wang, H., Garimella, S., and Murthy, J. (2007). Characteristics of an evaporating thin film in a microchannel. *Int. J. Heat Mass Transfer*, 50:3933–3942.

Wang, H., Garimella, S., and Murthy, J. (2008). An analytical solution for the total heat transfer in the thin-film region of an evaporating meniscus. *Int. J. Heat Mass Transfer*, 51:6317–6322.

Wang, H. S. and Rose, J. R. (2005). A theory of film condensation in horizontal noncircular section microchannels. *J. Heat Transfer*, 127:1096–1104.

Wang, H. S. and Rose, J. R. (2006). Film condensation in horizontal microchannels: effect of channel shape. *Int. J. Therm. Sci.*, 45:1205–1212.

Wang, H. S. and Rose, J. R. (2011). Theory of heat transfer during condensation in microchannels. *Int. J. Heat Mass Transfer*, 54:2525–2534.

Welch, S. W. J. and Radichi, T. (2005). Numerical computation of film boiling including conjugate heat transfer. *Numerical Heat Transfer*, Part B, 42:35–53.

Welch, S. W. J. and Wilson, J. (2000). A volume of fluid based method for fluid flows with phase change. *Journal of Computational Physics*, 170:662–682.

Weller, H. G., Tabor, G., Jasak, H., and Fureby, C. (1998). A tensorial approach to computational continuum mechanics using object-oriented techniques. *Computers in Physics*, 12:620–631.

Yaddanapudi, N. and Kim, J. (2001). Single bubble heat transfer in saturated pool boiling of FC-72. *Multiphase Sci. Technol.*, 12(3-4):47–63.